Thermal Effects in Ultrasonic Cavitation of Ionic Liquids

[1]Ross M. Elder; [1]Michael L. Calvisi*

[1]*University of Colorado, Colorado Springs, CO, USA*

Abstract

Ionic liquids have favorable properties for sonochemistry applications in which the high temperatures and pressures achieved by cavitation bubbles are important drivers of chemical processes. A model was developed to simulate ultrasonic cavitation in ionic liquids. The model uses the finite element method (FEM) and accounts for spatial variations in pressure and temperature in the interior and exterior of the bubble. This model provides insight into heat transfer across the bubble surface and thermal penetration into the liquid. Parametric studies are presented for sonochemistry applications involving ionic liquids as a solvent, examining a range of realistic ionic liquid properties to determine their effect on temperature and pressure inside the bubble and in the surrounding liquid. Results are presented for parametric variations including viscosity, thermal conductivity, and acoustic frequency. An additional study examines thermal penetration into the surrounding ionic liquid during bubble collapse. Among the most significant findings are that liquid viscosity and acoustic frequency have a strong effect on altering bulk and surface temperatures and pressures of the bubble. In all cases, the amount of thermal penetration into the exterior liquid is very small. Overall, the results suggest the prospect of tuning ionic liquid properties for specific applications.

Keywords: ultrasonic cavitation; sonochemistry; ionic liquids; heat transfer; finite element method

Introduction

Ionic liquids (ILs), salts that are liquid at or near room temperature, have favorable properties for chemical applications such as high thermal stability and negligible vapor pressure. ILs have been utilized for a variety of applications, including as catalysts and solvents for chemical reactions and ultrasonic cavitation [1]. In ultrasonic cavitation, diffuse acoustic energy is focused through the generation and oscillation of bubbles in a liquid, causing an oscillatory pressure and subsequent temperature rise in the liquid that can promote certain chemical reactions. Violent collapses, due to the nonlinearity of the bubble dynamics, can produce temperatures on the order of several thousand Kelvin and pressures on the order of several thousand atmospheres in the interior of the bubble [2]. While the massive temperatures tend to exist in a localized hot spot in the bulk of the bubble interior, the surrounding liquid may heat up significantly enough to undergo chemical reactions under the appropriate conditions.

ILs are comprised entirely of cations and anions, and the chemical structure has a strong influence on the thermophysical properties. As shown by Smiglak et al. [3], a variety of ILs can be combustible under significant heating due to their positive heats of formation, oxygen content, and decomposition products. While no research to our knowledge has stated the primary factors in producing a combustible IL, several ILs have been ignited, including protonated imidazolium nitrates, protonated C-nitro-substituted imidazolium nitrates and picrates, and 1-butyl-3 methylimidazolium azolates [3]. Others have been identified, synthesized, and characterized for propellant usage [4]. The combustibility of ILs presents a safety concern when performing acoustically-driven cavitation in ILs, due to the very large temperatures that can be exhibited in the interior of the bubbles. However, due to the competition between the time scales of motion and heat diffusion, the surrounding liquid may potentially experience little to no temperature change.

With over one trillion different IL possibilities [5], the potential for design freedom exists to tailor the cation and anion selection to yield favorable IL properties for a given application. To effectively utilize ILs in ultrasonic cavitation applications, it is important to understand how the liquid properties and system parameters affect the bubble dynamics, particularly the temperatures and pressures generated during collapse. To better understand this relationship, a numerical model of a spherical bubble was developed based on the finite element method (FEM). The state of the bubble interior during collapse is strongly influenced by several processes, including compressibility, surface tension, liquid viscosity, and heat transfer [2]. The numerical model accounts for all of these effects, in addition to spatial gradients in pressure and temperature throughout the flow domain. The model is used to conduct parametric studies on the effects of variations in acoustic frequency, IL viscosity, and IL thermal conductivity on the temperature and

*Corresponding Author, Michael L. Calvisi: mcalvisi@uccs.edu

pressures achieved in the bubble interior. This model is further used to study the effects of heat transfer through the bubble interior and into the surrounding IL, which provides insight into the feasibility of IL combustion.

Model Development

The object of interest is a single, spherical bubble surrounded by a Newtonian liquid driven by an acoustic standing wave. Because the bubble is spherical, the flow field is purely radial and therefore vorticity in the bubble wall region is considered negligible [6]. The bubble interior is initially composed of a noncondensable gas, such as argon, and potentially water vapor. The noncondensable gas is regarded as insoluble to the surrounding liquid based on the short time scale of the acoustic forcing, thus neglecting rectified diffusion. The outward flux of the noncondensable gas into the liquid has been shown by Storey and Szeri to have negligible effects on the bubble dynamics, unless at low ambient pressures [7]. Therefore, the number of moles of noncondensable gas present in the bubble interior is fixed throughout the entire oscillation. Additionally, the noncondensable gas and vapor are assumed to be inviscid. The model includes the effects of liquid viscosity, surface tension, and compressibility. The FEM model accounts for heat transfer throughout the bubble interior and exterior in the form of conduction and convection, but neglects mass transfer of water vapor at the bubble wall, which is beyond the scope of this paper. The physical processes of radiative heat transfer, light emission, chemical reactions, and buoyancy are neglected, as they are likely to have an insignificant effect on the results. The effects of shock waves are also not included in this study, for the diffusive transport in noble gas bubbles inhibits the steepening of wavy disturbances, such that shocks are not likely to occur inside argon bubbles [8, 9]. At cavitation collapse, though, the speed of the bubble wall can approach or surpass the speed of sound in the liquid. However, the total time the bubble wall is supersonic is a small fraction of the oscillation cycle; thus, the modeling error from neglecting shock waves in the liquid does not substantially affect the bubble dynamics [6].

COMSOL®, a commercial finite element software package, was used to develop the model. The program models a single, spherical bubble that undergoes a time and 1-D space-dependent change of volume in a compressible, Newtonian fluid at rest at an infinite distance relative to the initial bubble radius. The main bubble dynamics are described by laminar, two-phase compressible flow physics of immiscible fluids separated by a moving interface. A compressible formulation of the Navier-Stokes equations is implemented in both the interior and exterior domains. The velocity field, pressure field, and mesh deformation are solved for and the location of the interface is tracked by a deformed mesh. Upon post-processing, the Reynolds number of the simulations were shown to range from approximately 0.015 to 110, well within the laminar limit. The mesh nodes conform to the moving interface and other boundaries in the model. Regarding boundary conditions, a normal stress balance is applied at the gas-liquid interface to couple the separate Navier-Stokes equations used for the inner and outer domains. In addition, no-slip and kinematic boundary conditions are applied at the bubble surface so that it advects with the surrounding fluid. The outer liquid boundary is considered a pressure inlet to model the acoustic forcing. A sinusoidal pressure, $P_a = -A\sin(\omega t)$, is applied here through a Dirichlet boundary condition. The outer boundary wall is placed at 100 times the radius of the bubble in order to minimize numerical artifacts at the bubble surface due to the applied pressure at the outer boundary.

To account for heat transfer in the bubble interior, surrounding liquid, and fluid-fluid interface, transient conduction with pressure work, originating from the conservation of energy, was coupled to the Navier-Stokes equations. The pressure work term accounts for the heating of the fluids under adiabatic compression and thermoacoustic effects.

The FEM model above was validated against results in the literature, including those of Putterman and Weninger [10], and found to have good agreement. Due to the limited scope of this paper, further details are not included here.

Results

A baseline for the simulation parameters was determined. The IL 1-butyl-3-methylimidazolium tetrafluoroborate ([BMIM][BF4]) is one of the most commonly studied, commercially available ionic liquids and has been used experimentally in cavitation studies [11, 12]. Unlike many ILs, fluid property information for [BMIM][BF4] is readily available. Thus, the baseline fluid properties are chosen as those of [BMIM][BF4] at standard temperature and pressure. The bubble interior is assumed to consist of only the noncondensable gas argon. Water vapor can be present in the bubble interior if water is present or mixed with [BMIM][BF4], but consideration of the effects of water vapor is beyond the scope of the present study. Due to the low IL vapor pressure, the presence of IL vapor in the bubble interior can be neglected. The values selected for liquid and gas properties, and additional parameters are as follows:

ρ_l = 1201.2 kg/m^3, μ_l = 0.099200 Pa-s, σ_l = 0.045330 N/m, c_l = 1572.3 m/s, k_l = 0.18600 W/(m-K), $c_{p,l}$ = 1577.6 J/(kg-K), $T_{0,l}$ = 293.15 K, γ_g = 1.6700, k_g = 0.017574 W/(m-K), M_g = 0.039900 kg/mol, $c_{p,g}$ = 520.00 J/(kg-K), $T_{0,g}$ = 293.15 K, R_0 = 2.5-5.0 microns, P_∞ = 1.00 atm, T_∞ = 293.15 K, A = 1.10 atm, and f = 30.0 kHz, where ρ is density, μ is viscosity, σ is surface tension, c is speed of sound, k is thermal conductivity, c_p is specific heat, T is temperature, γ is ratio of specific heats, M is molecular weight, R is bubble radius, P is pressure, $f = \omega/2\pi$ is the acoustic forcing frequency, and the subscripts l, g, 0, and ∞ refer to the liquid, gas, initial state, and far-field, respectively. The initial bubble pressure is set so that it is in static equilibrium with the surrounding liquid.

Variation of Acoustic Frequency: To understand the effects of the wide range of frequencies that are commonly used for cavitation applications, the acoustic forcing frequency is varied in the range of 10-1000 kHz using the baseline parameters outlined above. For radii of 2.5, 5.0, and 15 μm, little change in temperature or pressure occurs with frequency. The temperature and pressure changes for the larger radii of 30 and 50 μm are much higher, and increase as frequency decreases. At lower frequencies, the forcing period is longer, which allows the bubble to expand to larger maximum radii and collapse to smaller minimum radii, thus increasing the compression ratio and, consequently, the maximum bulk temperatures and pressures achieved inside the bubble. All pressures approach the initial bubble pressure at the higher frequencies.

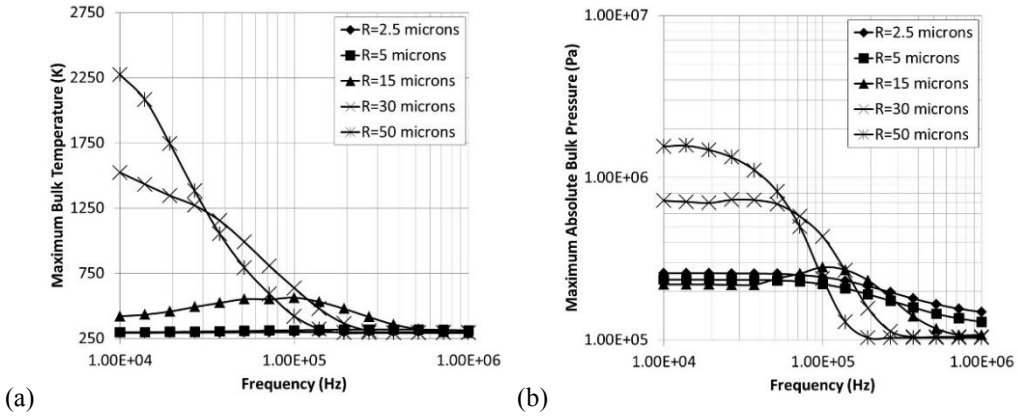

(a) (b)

Figure 1: (a) Maximum bulk temperature vs. frequency, and (b) maximum bulk pressure vs. frequency.

The surface temperature and pressure across the frequency range are shown in Figure 2. Despite the high temperatures at the center of the bubble, the bubble wall experiences significantly lower temperatures. The bubble wall also exhibits generally slightly higher maximum pressures than the bubble interior, typically occurring just after the point of minimum volume.

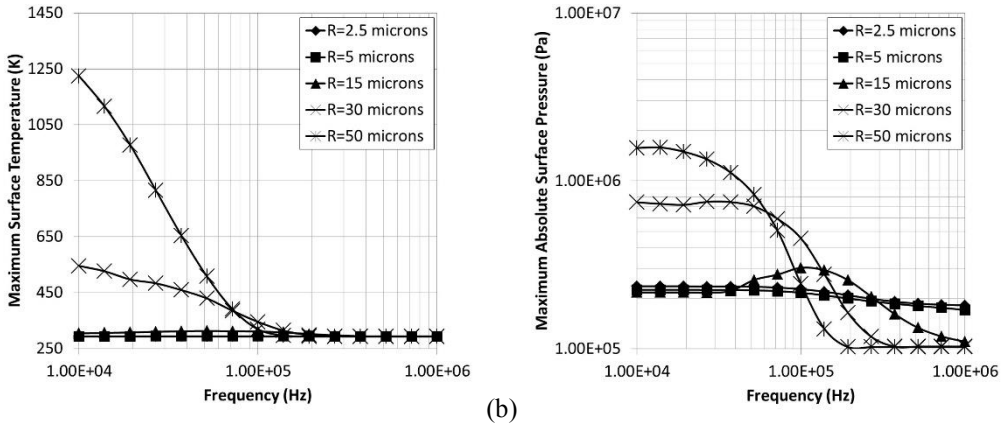

(a) (b)

Figure 2: (a) Maximum surface temperature vs. frequency, and (b) maximum surface pressure vs. frequency.

Variation of Viscosity: According to Endres et al. [13], ILs tend to exhibit viscosities within the range of 0.01-0.5 Pa-s compared to water, which has a viscosity of approximately 0.001 Pa-s at standard temperature and pressure. A larger range for ILs was stated by Wilkes [14] of 0.01-1 Pa-s. In order to understand the effect of viscosity, the viscosity was varied from 0.001-1 Pa-s. Although 0.001 Pa-s is not currently a feasible viscosity for an IL, further research may yield viscosities approaching this order of magnitude. The maximum bulk and surface temperature results are shown in Figure 3. Generally, as viscosity increases, the maximum temperatures decrease. Reducing viscosity yields a very significant increase in the temperatures achieved. As with lowering frequency, as the liquid viscosity decreases, the bubble achieves larger maximum radii and smaller minimum radii, thus increasing the compression ratio and, consequently, the maximum bulk temperatures achieved. Interestingly, one can see by comparing the bulk and surface temperature plots that for smaller initial radii, bubbles experience the largest temperature gradient from the center of the bubble to the wall. The time scales of collapse for the smaller bubbles are significantly shorter than that of the larger bubbles. This may potentially "trap" a larger portion of the heat at the center of the bubble, not allowing enough time for the heat to significantly diffuse through the bubble interior and through the bubble wall. This yields a larger temperature gradient for the smaller bubbles from the center to the liquid interface.

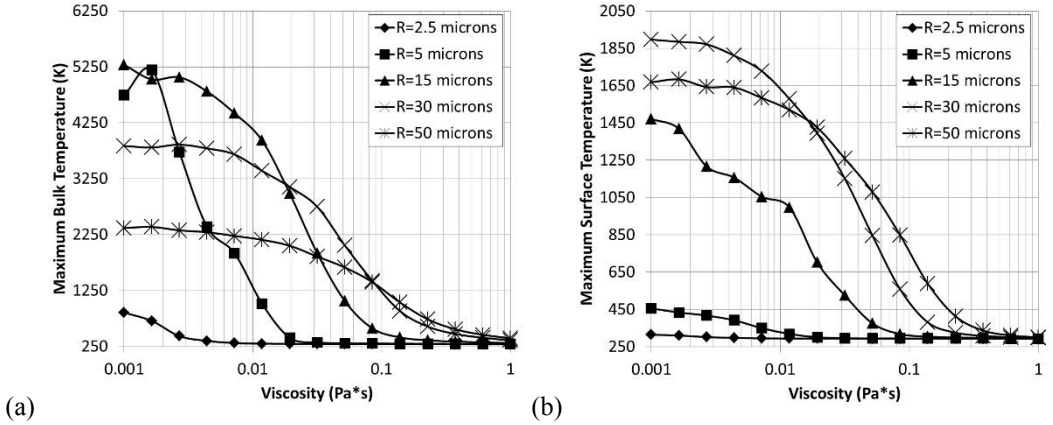

Figure 3: (a) Maximum bulk temperature vs. viscosity, and (b) maximum surface temperature vs. viscosity.

The maximum bulk pressure vs. viscosity is shown in Figure 4. Along with large bulk temperatures, the simulations demonstrate very high bulk pressures, some on the order of 1000 atm, which occurs at the deepest depths of the ocean. On a logarithmic plot, the surface pressures are not noticeably different from the bulk pressures and, hence, are not shown. The majority of these scenarios exhibit rather uniform pressures throughout the bubble interior. However, in some scenarios, there is as much as a 67% difference in pressure between the bubble center and wall.

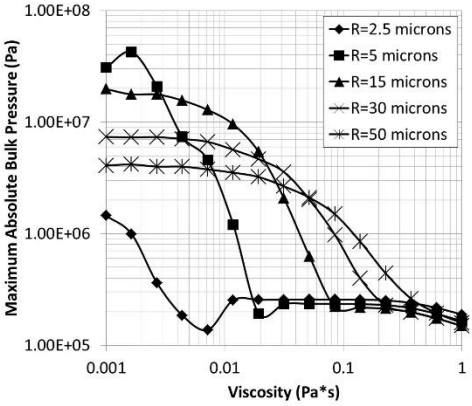

Figure 4: Maximum bulk pressure vs. viscosity.

Variation of Thermal Conductivity: While the results are not shown here for the sake of brevity, the simulations show that variations in IL thermal conductivity over a typical range of 0.1-0.5 W/(m-K) have a negligible effect on the bulk temperature. However, increasing thermal conductivity can significantly reduce the bubble surface temperature for initial radii equal to or greater than 30 microns. The larger thermal conductivity in the liquid promotes heat conduction away from the bubble, thereby lowering surface temperatures by as much as ~25% in these cases.

Thermal Penetration: As the above results show, the temperatures can decrease significantly from the bubble center to the surface. Several simulations were run, with the same baseline parameters as above, to determine the temperature gradient in the liquid and its penetration depth for varying parameters, including acoustic frequency, IL viscosity, and IL thermal conductivity. In the first study, the frequency of the acoustic forcing was varied from 10-1000 kHz. To compare the results of each scenario, the dimensionless volume of liquid heated as a function of the minimum heated dimensionless temperature (within that volume) is plotted in Figure 5 for initial radii of 5 and 30 microns, respectively, at the instant of minimum bubble volume. For an initial radius of 5 microns, decreasing the frequency to 10 kHz increases the bulk temperature and surface temperature greatly – as shown above – yet the liquid experiences much less of a temperature increase. The heat is transferred further into the liquid at the time of minimum volume, yielding higher volumes of heated liquid at the lower temperatures than other frequencies, but results in a much lower volume of higher temperature liquid. Furthermore, despite the high temperatures developed in the bulk, only a small liquid region experiences significant temperature change, with a maximum temperature increase of 83.2% for a 30 micron bubble at 10 kHz driving frequency.

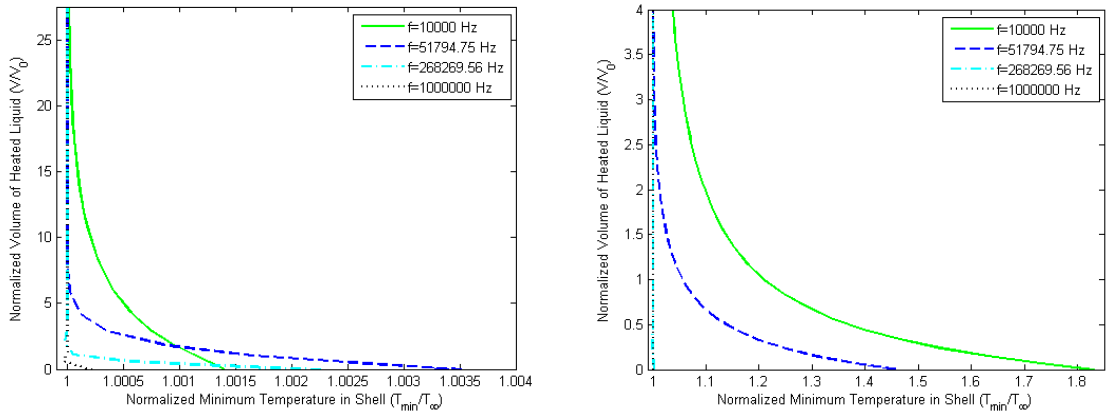

Figure 5: Dimensionless liquid volume heated vs. minimum dimensionless temperature at instant of minimum bubble volume with varying frequency. Left: R_0 = 5 microns. Right: R_0 = 30 microns.

Additional thermal penetration studies were performed by varying the IL viscosity from 0.001-0.5 Pa-s and the IL thermal conductivity over a typical range of 0.1-0.5 W/(m-K). Similar results were found; namely, the temperature increase in the liquid is relatively small – considering the large bulk temperatures achieved – and is confined to only a thin region around the bubble.

Conclusion

A model was developed to simulate ultrasonic cavitation in ionic liquids using the finite element method (FEM). Parametric studies were performed for sonochemistry applications involving ionic liquids as a solvent, examining a range of realistic ionic liquid properties to determine their effect on temperature and pressure inside the bubble and in the surrounding liquid. Results were presented for parametric variations including viscosity, thermal conductivity, and acoustic frequency. An additional study examined thermal penetration into the surrounding ionic liquid during bubble collapse. The results show that liquid viscosity and acoustic frequency have a strong effect on altering bulk and surface temperatures and pressures of the bubble. In all cases, the amount of thermal penetration into the exterior liquid is small relative to the initial bubble radius. Overall, the results suggest the prospect of tuning ionic liquid properties for specific applications.

References

[1] Calvisi, M. L., Lindau, O., Blake, J. R., Szeri, A. J. (2007). *Shape stability and violent collapse of microbubbles in acoustic traveling waves*. Phys. Fluids 19(047101).

[2] Storey, B. D., Szeri, A. J. (2001). *A reduced model of cavitation physics for use in sonochemistry*. Proc. R. Soc. Lond. 457.

[3] Smiglak, M., Reichert, W. M., Holbrey, J. D., Wilkes, J. S., Sun, L., Thrasher, J. S., Kirichenko, K., Singh, S., Katritzky, A. R., Rogers, R. D. (2006). *Combustible ionic liquids by design: Is laboratory safety another ionic liquid myth?* Chem. Commun.

[4] Sims, J., Forton, M., Allan, B., Rogers, R., Shamshina, J., Koelfgen, S. *Ionic liquids: Unlocking the gate to replacing hydrazine*. NASA Tech Briefs DRC-010-041.

[5] Forsyth, S. A., Pringle, J. M., MacFarlane, D. R. (2004). *Ionic liquids - An overview*, Aust. J. Chem. 57.

[6] Brenner, M. P., Hilgenfeldt, S., Lohse, D. (2002). *Single-bubble sonoluminescence*. Rev. of Modern Phys. 74.

[7] Storey, B. D., Szeri, A. J. (2000). *Water vapour, sonoluminescence and sonochemistry*. Proc. Math. Phys. Eng. Sci. 456(1999).

[8] Vuong, V. Q., Szeri, A. J. (1996). *Analytical integration and a numerical method for 1-D compressible flow with diffusive transport*. Computers and Fluids 25(1).

[9] Vuong, V. Q., Szeri, A. J. (1996). *Sonoluminescence and diffusive transport*. Phys. Fluids 8(9).

[10] Putterman, S. J., Weninger, K. R. (2000). *Sonoluminescence: How bubbles turn sound into light*, Annu. Rev. of Fluid Mech. 32(1).

[11] Flannigan, D. J., Hopkins, S. D., Suslick, K. S. (2005). *Sonochemistry and sonoluminescence in ionic liquids, molten salts, and concentrated electrolyte solutions*. J. Organometallic Chem. 10.

[12] Oxley, J. D., Prozorov, T., Suslick, K. S. (2002). *Sonochemistry and sonoluminescence of room-temperature ionic liquids*. J. Am. Chem. Soc. 125(37).

[13] Endres, F., Zein El Abedin, S. (2006). *Air and water stable ionic liquids in physical chemistry*, Phys. Chem. Chem. Phys. 8.

[14] Wilkes, J. S. (2004). *Properties of ionic liquid solvents for catalysis*. J. Molecular Catalysis A: Chem. 214.

© 2018 ASME